Coherent Exciton–Surface-Plasmon-Polariton Interaction in Hybrid Metal-Semiconductor Nanostructures

P. Vasa,[1,2] R. Pomraenke,[1] S. Schwieger,[2] Yu. I. Mazur,[3] Vas. Kunets,[3] P. Srinivasan,[4] E. Johnson,[4] J. E. Kihm,[5] D. S. Kim,[5] E. Runge,[2] G. Salamo,[3] and C. Lienau[1,*]

[1]*Institut für Physik, Carl von Ossietzky Universität, D-26111 Oldenburg, Germany*
[2]*Technische Universität Ilmenau, Fachgebiet Theoretische Physik I, Postfach 100565, D-98684 Ilmenau, Germany*
[3]*Department of Physics, University of Arkansas, Fayetteville, Arkansas 72701, USA*
[4]*The Center for Optoelectronics and Optical Communications, University of North Carolina at Charlotte, Charlotte, North Carolina 28223, USA*
[5]*School of Physics, Seoul National University, Seoul 151-742, Korea*

(Received 18 December 2007; revised manuscript received 1 August 2008; published 8 September 2008)

We report measurements of a coherent coupling between surface plasmon polaritons (SPP) and quantum well excitons in a hybrid metal-semiconductor nanostructure. The hybrid structure is designed to optimize the radiative exciton-SPP interaction which is probed by low-temperature, angle-resolved, far-field reflectivity spectroscopy. As a result of the coupling, a significant shift of ~ 7 meV and an increase in broadening by ~ 4 meV of the quantum well exciton resonance are observed. The experiments are corroborated by a phenomenological coupled-oscillator model predicting coupling strengths as large as 50 meV in structures with optimized detunings between the coupled exciton and SPP resonances. Such a strong interaction can, e.g., be used to enhance the luminescence yield of semiconductor quantum structures or to amplify SPP waves.

DOI: 10.1103/PhysRevLett.101.116801 PACS numbers: 73.20.Mf, 71.35.Gg, 78.67.De

The radiative coupling between an emitter and its electromagnetic environment gives rise to fundamental quantum-optical phenomena like vacuum Rabi or normal mode splittings [1–3] and the Purcell effect [4]. Modifications of the spontaneous emission due to radiative coupling have been demonstrated for various quantum systems ranging from single atoms [1] to semiconductor quantum dots [2] and quantum wells (QW) [3,5] coupled to a microcavity. Many groups have investigated similar interactions in close proximity of metallic structures [6,7]. Various experimental [8–10] and theoretical [6,11] studies have shown an enhancement in the luminescence yield as well as a reduction of the excitonic lifetime of a QW when placed close to a metallic nanostructure due to its coupling to surface plasmon polaritons (SPPs). Other reports, however, show a suppression of luminescence in the proximity of a metal surface [12,13]. The discussion of these results has partly remained controversial because present experiments give limited insight into the microscopic nature of the coupling. Hence the interaction between a metallic nanostructure and a quantum emitter is not fully understood. One of the most direct ways to probe this interaction is to study the normal mode splitting between QW excitons and SPP.

In this Letter, we investigate the linear optical properties of a hybrid nanostructure consisting of a GaAs QW placed in the vicinity of a metallic nanoslit array [14,15]. We report the first direct observation of the normal mode splitting between QW excitons and SPPs in the nanoslit array. As a result of this coupling, low-temperature angle-resolved far-field reflectivity spectra reveal a significant shift in the exciton resonance position together with an increase in the radiative exciton damping.

We investigate a multilayer, metal-semiconductor hybrid structure consisting of a gold nanoslit grating deposited on a GaAs/AlGaAs QW heterostructure. The sample consists of a 10 nm wide GaAs QW layer embedded in $Al_{0.3}Ga_{0.7}As$ barriers grown by molecular beam epitaxy on a GaAs substrate. On the top side, the barrier has a height of only 20 nm and is capped by a 3 nm GaAs buffer to ensure that the QW is close to the surface while maintaining sufficient optical quality. A $h = 80$ nm thick gold film is then deposited on the top surface of the semiconductor. Then an array of $d = 140$ nm wide slits with a grating period of $a_0 = 500$ nm is created by electron beam lithography. A schematic of the sample cross section and a scanning electron microscope image of the top surface are shown in Figs. 1(a) and 1(b), respectively. Such a nanoslit grating is chosen (i) because these arrays provide a particularly efficient coupling between SPP and far-field radiation and (ii) because its linear optical properties are now reasonably well understood [14,15].

In our experiments such a nanoslit array is illuminated with p-polarized light, with its electric field vector perpendicular to the slit axis. In this case, SPPs are excited at both air-metal (AM) and semiconductor-metal (SM) interfaces by transferring momentum $n\frac{2\pi}{a_0}$, $n \in \mathbb{Z}$, to the incident photons. Angle-dependent reflectivity spectra of such nanoslit arrays reveal the excitation of different AM and SM resonances as illustrated in the simulations shown in Fig. 1(c). The hybrid structure parameters are chosen similar to our sample and the spectra have been calculated

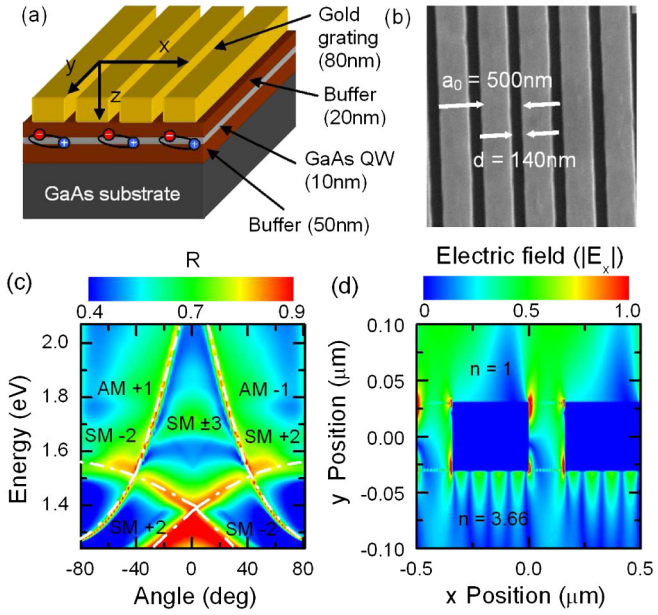

FIG. 1 (color online). (a) Schematic of the metal-semiconductor hybrid structure consisting of a gold nanoslit grating deposited on a GaAs QW. (b) Scanning electron microscope image of the gold grating with $a_0 = 500$ nm, $d = 140$ nm, and $h = 80$ nm. (c) Calculated angle-resolved far-field reflectivity spectra of this structure. Dispersion relations for different AM and SM SPP resonances are indicated as dash-dotted lines. (d) Calculated spatial distribution of the normal electric field E_x for $E_{ex} = 1.517$ eV and $\theta = 38°$, near the crossings of the SM[+2], SM[−3], and AM[−1] SPP resonances.

using a full vectorial diffraction model [15,16] by assuming a spatially homogeneous refractive index $n_s = 3.66$ of the semiconductor layers. The spectra indicate that at excitation energies of ~1.5 eV, i.e., around the exciton resonance of a 10 nm GaAs QW and at an incidence angle $\theta = 40°$, three different SPP modes, AM[−1], SM[+2], and SM[−3], are almost in resonance leading to an efficient coupling among these modes via the light transmitted through the nanoslits.

In Fig. 1(d), the spatial distribution of the electric field component E_x perpendicular to the slit axis is shown for illumination by a p-polarized monochromatic plane wave with $E_{ex} = 1.517$ eV, incident at $\theta = 38°$. This is close to the crossing of the SM[−3], SM[+2], and AM[−1] SPP resonances. The calculations indeed reveal the formation of coupled SPP modes with spatially localized field intensities at both the AM and SM interfaces. Inside the semiconductor, the SPP fields are characterized by a short modulation period along x of $a_0/|2n| \sim 100$ nm due to the dominant contribution from the $n = +2$ and -3 diffraction orders. The SPP field is mostly evanescent with a decay length of only ~50 nm, due to the large n_s of the semiconductor. When placed within this decay length, the transition dipole moment of the QW exciton couples to this strong evanescent field.

Both the SPP field at the SM interface and the electric field emitted by the QW are coupled via the nanoslits to evanescent SPP fields at the AM interface. Therefore they are rescattered into propagating radiation [14,15] and can be detected in the far field in a reflection geometry. It is, however, not necessarily needed for observing exciton-SPP couplings. The parameters of our sample are chosen so that the heavy hole (HH) and light hole (LH) exciton resonances of the QW at a temperature of $T = 10$ K occurring at 1.546 and 1.554 eV, respectively, match well with the coupled AM-SM resonance. A strong exciton-SPP interaction is expected only in a narrow range of incidence angles, when the almost dispersionless QW exciton and the highly angle-dependent SPP are brought into resonance.

To study this interaction, the sample is illuminated in the energy range between 1.503 and 1.569 eV with a weakly focused p-polarized beam from a tunable continuous wave Ti:sapphire laser. Angle-resolved, linear reflectivity spectra are recorded for $\theta = 26°$–$44°$ at $T = 10$ K with an angular resolution of 0.2° and a spectral resolution of 0.2 meV [Fig. 2(a)]. The spectra are almost entirely dominated by the strong reflectivity peak of the SPP resonance resulting from the coupling among the AM[−1], SM[+2], and SM[−3] modes. This resonance is highly dispersive and is essentially unaffected by the presence of the QW. Very faint features from the QW and GaAs substrate (at 1.512 eV) resonances are also visible. As expected the QW signature is weak, since most of the incident light is simply reflected off the metal grating.

We expect that the weak QW signal has little effect on the strong SPP peaks in the reflectivity spectra. Therefore more detailed information on the QW reflectivity can be obtained by subtracting the contribution from the SPP resonance from the data. Recent studies on metallic nanoarrays have shown that SPP line shape is well described by a Fano-like line shape [14,17] given by $R(\omega, \theta) = |r(\omega, \theta)|^2$ with

$$r(\omega, \theta) = a + \frac{b\Gamma}{\omega - \omega_{\mathrm{SPP}}(\theta) + i(\gamma + \Gamma)}. \qquad (1)$$

Here, a and b are frequency-independent complex amplitudes and $\omega_{\mathrm{SPP}}(\theta)$ is the SPP resonance frequency. The nonradiative SPP damping rate is given by γ, whereas Γ is the dominant radiative damping rate [14,18].

In agreement with previous work, this Fano model satisfactorily describes the experimental line shapes [Fig. 2(a)]. The parameters of the model, i.e., the dispersion $\omega_{\mathrm{SPP}}(\theta)$ of the coupled SPP resonance and the linewidth $\gamma + \Gamma$, agree well with our model calculations [4]. The SPP dispersion is mainly given by that of the AM[−1] resonance.

Difference spectra obtained by subtracting these simulations from the original data are shown in Fig. 2(c). We observe a small remaining signature of the strongly dispersive SPP, a distinct LH exciton resonance at around 1.554 eV, a HH exciton resonance at 1.546 eV, and the

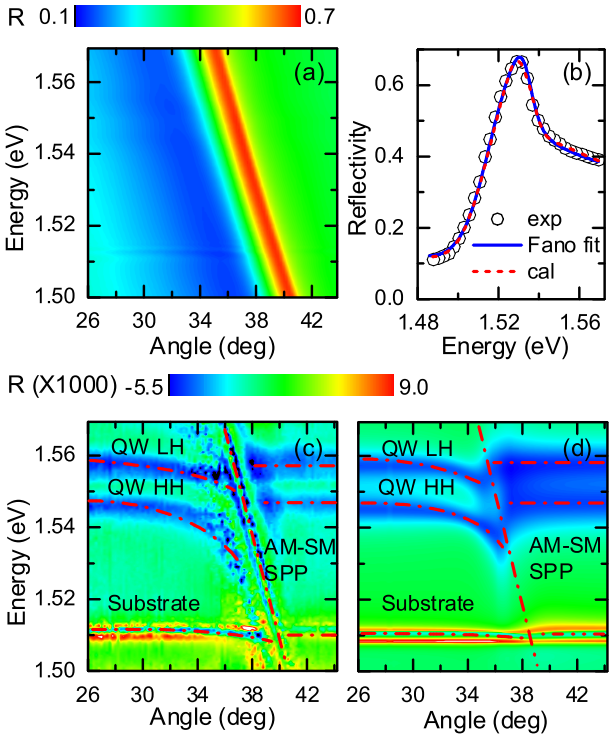

FIG. 2 (color online). (a) Angle-resolved reflectivity spectra ($T = 10$ K) of the hybrid structure. The dominant feature is the resonance resulting from the coupling of the AM[−1], SM[+2], and SM[−3] SPP modes. (b) Spectrum at $\theta = 38°$ (open circles) together with simulations based on the Fano (blue solid line) and the coupled-oscillator model (red dashed line). (c) Reflectivity spectra obtained after subtracting the SPP contribution from (a). The spectra reveal a clear shift of the HH and LH QW resonances. (d) Spectra obtained from the coupled-oscillator model. Red dash-dotted lines indicate the SPP and QW HH and LH dispersions, respectively.

excitonic excitation of the GaAs substrate at 1.512 eV. The substrate feature is split into two closely spaced narrow resonances reflecting a minor strain-induced lifting of the degeneracy of LH and HH excitons. Their resonance energies are mainly unchanged when varying θ. In contrast, for the QW excitonic transitions we observe a clear bending of both QW LH and HH resonances together with a slight increase in broadening near the crossing with the SPP resonance. The changes in line position and width are a clear signature of exciton-SPP coupling in hybrid metal-semiconductor nanostructures.

To quantitatively explain the SPP-QW interaction, a phenomenological model is used, in which the AM[−1], SM[+2], and exciton resonances are treated as three coupled Lorentzian oscillators. Such a classical coupling model is commonly used to study normal mode splittings in various systems because the dispersion relations of the coupled modes are mainly affected by the quantum properties of the emitters [19,20].

As a first approximation, the SPP couplings of HH and LH excitons are treated separately because of their sufficiently different energies. For each excitonic resonance the reflectivity spectrum is modeled by a function of the form of Eq. (1), but now with three Lorentzian oscillators instead of one. The uncoupled SPP and exciton resonances are represented by a diagonal matrix H_{uc} where the complex entries V_{ii} are $\omega_i - i\Gamma_i$, with $i = 1$ corresponding to AM[−1], $i = 2$ to SM[+2], and $i = 3$ to the QW HH, LH or substrate exciton with known dispersion relations. The total matrix for the coupled system is given as

$$H_{uc} + H_c = \begin{pmatrix} V_{11} & 0 & 0 \\ 0 & V_{22} & 0 \\ 0 & 0 & V_{33} \end{pmatrix} + \begin{pmatrix} 0 & V_{12} & 0 \\ V_{21} & 0 & V_{23} \\ 0 & V_{32} & 0 \end{pmatrix}. \quad (2)$$

In H_c, the parameters V_{ij} are complex coupling elements. $V_{12} = V_{21}$ denotes the slit-induced coupling between AM[−1] and SM[+2] SPPs [14,15]. The parameters $V_{23} = V_{32}$ denote the coupling between the exciton and the SM[+2] SPP. This reflects the coupling $\vec{\mu} \cdot \vec{E}_{\mathrm{SPP}}$ between the exciton dipole moment $\vec{\mu}$ and the local SPP field. Under our weak excitation conditions $\vec{E}_{\mathrm{SPP}}$ is dominated by the *vacuum* SPP field, as in previous experiments [2,3]. In our structure there is no direct coupling between air side plasmons and the QW [$V_{13} = V_{31} = 0$].

Eigenvalues of this coupled matrix are used to calculate $R(\omega, \theta)$. The calculated spectra compare well with the experimental data [Fig. 2(b)]. To compare with Fig. 2(c), the SPP contribution is subtracted from the simulated $R(\omega, \theta)$ and the resulting QW dispersion is illustrated in Fig. 2(d). Satisfying agreement with experiment is obtained for the following coupling parameters: $V_{12} = (90 + 30i)$ meV, $V_{23}^{\mathrm{LH}} = (40 + 5i)$ meV, $V_{23}^{\mathrm{HH}} = (-50 - 6i)$ meV, and $V_{23}^{\mathrm{sub}} = (-18 - 2i)$ meV [Fig. 3(a)]. Because of the considerable field enhancement in the metallic slit structures, these values for the coupling strengths are larger than in many dielectric microcavities.

The model correctly predicts various salient features of our measurements. Most importantly, it reproduces the strongly asymmetric shift of the QW resonances seen in Fig. 3(b). This shows that the QW exciton is coupled to at least two interacting SPP modes. For small angles ($\theta < 36°$), these two modes interact constructively, giving rise to a large spectral shift. On the high-angle side, destructive interference diminishes the exciton-SPP interaction. The model also explains why the observed shift of 6–8 meV is much smaller than the predicted coupling strengths of ~50 meV. In our structure the crossing between the AM and SM modes is not perfectly matched to the exciton-SPP resonance. This off-resonance condition reduces the effective coupling strength significantly. In Fig. 3(b), the shift of the LH resonance is less pronounced than the HH shift. This obviously reflects the larger in-plane component of the HH dipole moment $\vec{\mu}_{\parallel}$ and shows that the coupling is induced by the in-plane components of the SPP field. The very small shift of the substrate resonance evidently reflects its large spatial separation from the interface. This

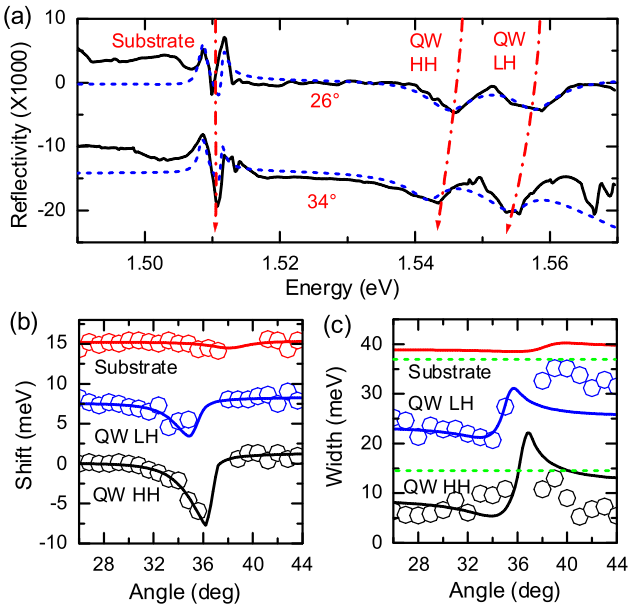

FIG. 3 (color online). (a) Experimental (black solid lines) and simulated (blue dashed lines) reflectivity spectra at $\theta = 26°$ and 34°, respectively. The red dash-dotted lines are guides to the eye. (b),(c) Experimental (open circles) and simulated (lines) energy shifts (b) and line widths (c) of the LH (blue), HH (black), and substrate (red) excitonic resonances as a function of angle θ. The LH and substrate transitions are vertically shifted for clarity. In (c), the green dashed lines mark the new reference positions.

results in a reduced spatial overlap with *evanescent* SPP fields [Fig. 2(d)] which cause the exciton-SPP coupling.

The results in Fig. 3(c) show a rather surprising angle-dependent change in the linewidth of the exciton resonances. The HH resonance width changes from a nearly constant width of ~6 meV to about 10 meV when brought into resonance with the SPP mode. This means that the on-resonance linewidth is not purely given by the predominantly inhomogeneous broadening of the QW exciton line, but that the coupling to SPP induces an additional, and surprisingly strong, radiative damping of the coherent exciton polarization.

This is of interest because it means that the radiative damping time of a quantum emitter can be decreased to values of few ps or even below by coupling it to SPP in metal nanoslit arrays, provided that (i) its emission energy is in resonance with the SPP excitation and (ii) its dipole moment is appropriately aligned to strongly couple to the SPP modes. In such arrays SPP excitations are predominantly radiatively damped [$\Gamma \gg \gamma$ in Eq. (1)] [14,18]. Therefore the luminescence efficiency of an emitter with a low quantum yield (e.g., carbon nanotubes) can be enhanced by coupling its emission via the SPP excitations into the far field. In contrast, metal structures with dominant nonradiative damping ($\Gamma < \gamma$) [12,13] will reduce the luminescence yield. Of course for emitters with an inherently large quantum yield, such as excitons in the GaAs QW studied here, only minor enhancements of the luminescence yield are possible.

In conclusion, we have investigated for the first time the coherent interaction between quantum well excitons and surface plasmon polaritons in a novel hybrid metal-semiconductor nanostructure. This coupling gives rise to spectral shifts of the exciton resonance and to a surprising increase in the radiative exciton damping. Our results present a quantitative measure of the coupling strength and show that couplings as large as 50 meV can be reached in samples with optimized geometries. Because of the large optical nonlinearities of QW excitons, such a strong exciton-SPP coupling [21] is of considerable interest for various future applications. This strong coupling may be beneficial for enhancing the quality factor of metallic nanoresonators by SPP amplification [22,23], or it may help to build SPP lasers [22] and to transfer quantum information over mesoscopic distances.

We gratefully acknowledge helpful discussions with Q. H. Park (Seoul) and C. Ropers (Berlin). We thank Alexander von Humboldt Foundation (P. V.) and DFG (SFB 296) for financial support.

*christoph.lienau@uni-oldenburg.de

[1] T. J. Thompson, G. Rempe, and H. J. Kimble, Phys. Rev. Lett. **68**, 1132 (1992).
[2] T. Yoshie *et al.*, Nature (London) **432**, 200 (2004).
[3] C. Weisbuch, M. Nishioka, A. Ishikawa, and Y. Arakawa, Phys. Rev. Lett. **69**, 3314 (1992).
[4] E. M. Purcell, Phys. Rev. **69**, 681 (1946).
[5] J. M. Gerard *et al.*, Phys. Rev. Lett. **81**, 1110 (1998).
[6] K. X. Drexhage *et al.*, *Progress in Optics* (North Holland, Amsterdam, 1974), Vol. 12, p. 165.
[7] I. Pockrand, A. Brillante, and D. Moebius, J. Chem. Phys. **77**, 6289 (1982).
[8] N. E. Hecker, R. A. Hoepfel, and N. Sawaki, Physica (Amsterdam) **2E**, 98 (1998).
[9] K. Okamoto *et al.*, Nature Mater. **3**, 601 (2004).
[10] Y. Fedutik *et al.*, Phys. Rev. Lett. **99**, 136802 (2007).
[11] W. Zhang, A. O. Govorov, and G. W. Bryant, Phys. Rev. Lett. **97**, 146804 (2006).
[12] I. Gontijo *et al.*, Phys. Rev. B **60**, 11 564 (1999).
[13] A. Neogi *et al.*, Phys. Rev. B **66**, 153305 (2002).
[14] C. Ropers *et al.*, Phys. Rev. Lett. **94**, 113901 (2005).
[15] K. G. Lee and Q. H. Park, Phys. Rev. Lett. **95**, 103902 (2005).
[16] H. Lochbihler, Phys. Rev. B **50**, 4795 (1994).
[17] C. Genet, M. P. van Exter, and J. P. Woerdman, Opt. Commun. **225**, 331 (2003).
[18] D. S. Kim *et al.*, Phys. Rev. Lett. **91**, 143901 (2003).
[19] R. Houdré *et al.*, Phys. Rev. Lett. **73**, 2043 (1994).
[20] D. G. Lidzey *et al.*, Nature (London) **395**, 53 (1998).
[21] J. Dintinger *et al.*, Phys. Rev. B **71**, 035424 (2005).
[22] D. J. Bergman and M. I. Stockman, Phys. Rev. Lett. **90**, 027402 (2003).
[23] J. Seidel, S. Grafstroem, and L. Eng, Phys. Rev. Lett. **94**, 177401 (2005).